RESEARCH ARTICLE

Applied Organometallic Chemistry WILEY

Computational design and characterization of platinum-II complexes of some Schiff bases and investigation of their anticancer–antibacterial properties

Serpil Kaya [ID] | Sultan Erkan [ID] | Duran Karakaş [ID]

Science Faculty, Chemistry Department, Cumhuriyet University, Sivas, Turkey

Correspondence
Duran Karakaş, Cumhuriyet University, Science Faculty, Chemistry Department, 50140, Sivas, Turkey.
Email: dkarakas@cumhuriyet.edu.tr

Abstract

$Pt(L_1)_2$-, $Pt(L_2)_2$-, and $Pt(L_3)_2$-type four-coordinated hypothetical platinum-II complexes were designed and characterized computationally. Where L_1, L_2, and L_3 are the Schiff base anions as 2-((ethylamino)methyl)-6-methoxyphenolate, 2-((ethylamino)methyl)-6-methylphenolate, and 2-((ethylamino)methyl)-6-chlorophenolate, respectively. M062X/LANL2DZ/6-31G(d,p) level was found to be the best computational level for the complexes by benchmarking analysis. $Pt(L_n)_2$-type four-coordinated complexes were optimized in the aqueous phase at the best level. Spectroscopic properties of optimized molecular structures (IR, ^{1}H-NMR, ^{13}C-NMR, and UV–Vis) were calculated, and the complexes were characterized. It was determined that $Pt(L_n)_2$-type complexes have a distorted square planar geometry. Molecular electrostatic potential maps, molecular orbital energy diagrams, and some molecular properties of the complexes were calculated. To estimate the anticancer and antibacterial activities of the complexes, they were docked against Michigan Cancer Foundation-7 (MCF7) and *Mycobacterium tuberculosis* (H37Rv) cell lines and compared with standard substances. According to the calculated docking parameters, the complexes were found to have higher activity than substances with anticancer and antibacterial standards. The presence of an electron-donating group in Schiff bases has been predicted to increase both anticancer and antibacterial activities.

Highlights

- $Pt(L_1)_2$, $Pt(L_2)_2$, and $Pt(L_3)_2$ complexes were designed and optimized at the M062X/LANL2DZ/6-31G(d,p) level.
- The complexes were characterized by molecular structure parameters, IR, nuclear magnetic resonance (NMR), and UV–Vis spectroscopic data and were found to have distorted square planar geometry.
- The antitumor-antibacterial activity of the $Pt(L_3)_2$ complex was predicted to be higher than the references and the HL_3 ligand.

KEYWORDS

antibacterial activity, anticancer, computational chemistry, platinum complexes, Schiff bases

1 | INTRODUCTION

Imines, also known as azomethine or Schiff bases, have the general formula $R_1R_2C=NR_3$ ($R_3 \neq H$).[1] In the given general formula, the R_1, R_2, and R_3 groups may be alkyl, aryl, cycloalkyl, or heteroaryl. The size of these groups, electron-withdrawing or electron-donating, has a significant effect on the physical and chemical properties of Schiff bases. Schiff bases are stable compounds that can be synthesized from the reaction of aldehydes or ketones with primary amines.[2] Such compounds are widely used for industrial purposes such as pigment, catalyst, and chemical additives.[3] Additionally, it is known that such compounds exhibit pharmacological activities such as antimicrobial, antifungal medications, antitumor, antimalarials, antiproliferative, anti-inflammatory, antiviral, and antipyretic.[2,4–7]

Schiff bases are widely used ligands in complex chemistry.[8] The imine nitrogen in these ligands is basic and is in the π-acceptor ligand class. Schiff bases donate the electron pair on the nitrogen atom to the metal ion and form a σ bond and take electrons from the metal ions to the π* orbital of azomethine group to form a π bond.[9] Schiff bases can act as a bidentate ligand if they contain a proton-donating functional group close to the imine group.

Schiff base complexes could be easily synthesized when Schiff bases and metal salts are reacted under mild conditions.[10] It can be said that factors such as the type of metal ion, size, charge, coordination number, and properties of Schiff base are highly effective on the stability and biological activity of Schiff base metal complexes.[11] In general, Schiff base complexes represent an important group of compounds of biological importance. There are many published articles on Schiff base metal complexes showing antibacterial, antifungal, and anticancer activity.[12–23]

Cisplatin-based complexes such as carboplatin, nedaplatin, oxaliplatin, lobaplatin, and heptaplatin are widely used in the treatment of various cancer types such as ovarian, testicular, bladder, colorectal, lung and head, neck, pancreatic, gastric, and breast cancer.[24] However, cisplatin therapy has serious side effects such as nephrotoxicity, cumulative peripheral sensory neuropathy, ototoxicity due to irreversible damage to hair cells, and nausea and vomiting.[25–27] For these reasons, studies are underway to develop other platinum-based antitumor drugs.

In our previous study, we designed HL_1, HL_2, and HL_3 Schiff base ligands; characterized them by calculating their IR, ^{1}H-NMR, ^{13}C-NMR, and UV–Vis spectra; and estimated their anticancer–antibacterial activities.[9] The aim of this study is to design platinum-II complexes of L_1, L_2, and L_3 Schiff base anions, to characterize them with quantum chemical calculations, and to predict their anticancer–antibacterial activities. For this purpose, $Pt(L_1)_2$-, $Pt(L_2)_2$-, and $Pt(L_3)_2$-type four-coordinated hypothetical complexes were designed. The ground state structures of the complexes were optimized at M062X/LANL2DZ/6-31+G(d,p) level in the aqueous phase. These structures were characterized by calculating IR, nuclear magnetic resonance (NMR), and UV–Vis spectra. The complexes were docked against the MCF7 and the H37Rv cell lines to predict their anticancer and antibacterial activities, and the docking results were compared with standard substances.

2 | METHODS AND TECHNIQUES

Schematic structures of Pt $(L_n)_2$-type Schiff base complexes were designed in GaussView 6.0.16 program.[28] Optimized structures and vibrational frequency of complexes were obtained at M062X/LANL2DZ/6-31+G(d,p) level in Gaussian 09: AS64L-G09RevD.01 program in the aqueous medium, and no imaginary vibrational frequency was observed within the calculated frequencies.[29,30] M062X method is a hybrid method based on density functional theory. This method defines the exchange-correlation energy functional based on the meta-GGA approximation.[31] LANL2DZ/6-31+G(d,p) is a mixed basis set.[32] LANL2DZ basis set uses an internal potential for the nucleus and inner shell electrons, and this basis set is often used for post-third-order atoms.[33] 6-31+G(d,p) is a basis set with diffuse-functional that adds d-functions to heavy atoms and p-functions to hydrogen atoms.[32]

Chemical events taking place in living beings are generally in the aqueous environment. Therefore, computations on Pt $(L_n)_2$-type complexes were performed in the water medium by using conductor-like polarizable continuum model (C-PCM).[34] NMR spectra were computed with the gauge-independent atomic orbitals (GIAO) method,[35] and UV–Vis spectra were calculated with the time-dependent-density functional theory (TD-DFT) method.[36] Mean molecular polarizability (α), static dipole moment (μ), energy of the HOMO (E_{HOMO}), and energy of the LUMO (E_{LUMO}) were taken from the calculation output file. Some molecular properties such as ionization potential (I), electron affinity (A), between LUMO and HOMO energy gap (ΔE), hardness (η), absolute electronegativity (χ), and electrophilicity index (ω) of the complexes were obtained from Equations 1–6.[9]

$$I = -E_{HOMO} \tag{1}$$

$$A = -E_{LUMO} \tag{2}$$

$$\Delta E = E_{LUMO} - E_{HOMO} \tag{3}$$

$$\eta = I - A/2 \tag{4}$$

$$\chi = I + A/2 \tag{5}$$

$$\omega = \mu_{cp}^2/2\eta \tag{6}$$

Both Pt $(L_n)_2$-type complexes and the antitumor standard cisplatin were docked against the MCF-7 (PDB ID: 1JNX) cell line.[37] Additionally, Schiff base complexes and antibacterial reference N-(Salicylidene)-2-hydroxyaniline (SHA)[2] were docked against the H37Rv (PDB ID: 3TZ6) tuberculosis bacterial cell line.[38] Docking server was used in molecular docking calculations.[39]

3 | RESULTS AND DISCUSSION

3.1 | Determination of the best calculation level

Method and basis set selection has an important role in computational studies. For this purpose, taking into account the molecule whose properties will be calculated, different levels are created. At the levels created, a measured property of the molecule is calculated. The compatibility between the calculated and the measured feature is analyzed. The level that provides the best fit is taken into account as the best calculation level. This process is called benchmark analysis. There is no

experimental data in the literature for the Pt $(L_n)_2$-type complexes designed in this study. However, some molecular structure parameters of Ni $(L_n)_2$ [bis(N-R-1-naphthylethyl-3,5-dichlorosalicydenaminato)nickel (II)] complex, which has a similar structure to Pt $(L_n)_2$ complexes, are given in the literature.[40] The level that gives the correct parameters for Ni $(L_n)_2$ can also be used for Pt $(L_n)_2$-type complexes. Therefore, the Ni-N, Ni-O, C=N bond lengths and N-Ni-O(1), N-Ni-O(2) bond angles of the Ni $(L_n)_2$ complex were computed at the levels of HF/LANL2DZ/6-31G **(1)**, HF/LANL2DZ/6-31G(d) **(2)**, HF/LANL2DZ/6-31G+(d,p) **(3)**, B3LYP/LANL2DZ/6-31G **(4)**, B3LYP/LANL2DZ/6-31G(d) **(5)**, B3LYP/LANL2DZ/6-31G+(d,p) **(6)**, M062X/LANL2DZ/6-31G **(7)**, M062X/LANL2DZ/6-31G(d) **(8)**, and M062X/LANL2DZ/6-31+G(d,p) **(9)**. The calculated values of the mentioned bond lengths and bond angles are presented in Table 1 together with their experimental values.

The mean of the differences between the calculated and the experimental values can be taken as a benchmark. Therefore, the mean of differences was calculated from Equation 7 and given in the last column of Table 1.

$$MD = \frac{|C - E|}{N} \tag{7}$$

Here, MD is the mean of differences, C is the calculated value, E is the experimental value, and N is the number of values. The level with the MD value closest to zero can be taken as the most appropriate level. As can be seen from Table 1, the level with the MD value closest to zero is **(9)**. Therefore, M062X/LANL2DZ/6-31+G(d,p) level was chosen for Pt $(L_n)_2$-type complexes in this study.

TABLE 1 Some bond lengths (Å) and bond angles (°) of the Ni $(L_n)_2$ complex calculated at various levels

Level	Bond lengths (Å)			Bond angles (°)		MD
	Ni-N	Ni-O	C=N	N-Ni-O(1)[a]	N-Ni-O(2)[a]	
(1)	2.010	1.863	1.280	89.9	90.0	0.823
(2)	2.024	1.867	1.272	90.7	89.3	0.528
(3)	2.026	1.872	1.272	90.7	89.3	0.529
(4)	1.948	1.856	1.308	92.3	87.9	0.115
(5)	1.954	1.851	1.298	92.4	87.5	0.213
(6)	1.957	1.860	1.298	92.3	87.6	0.175
(7)	1.965	1.853	1.297	91.6	88.0	0.155
(8)	1.972	1.852	1.288	92.3	87.7	0.155
(9)	1.937	1.847	1.281	92.2	87.8	0.105
Exp.	1.936	1.823	1.280	92.1	88.2	

[a]O(1) and O(2) were defined in Figure 1.
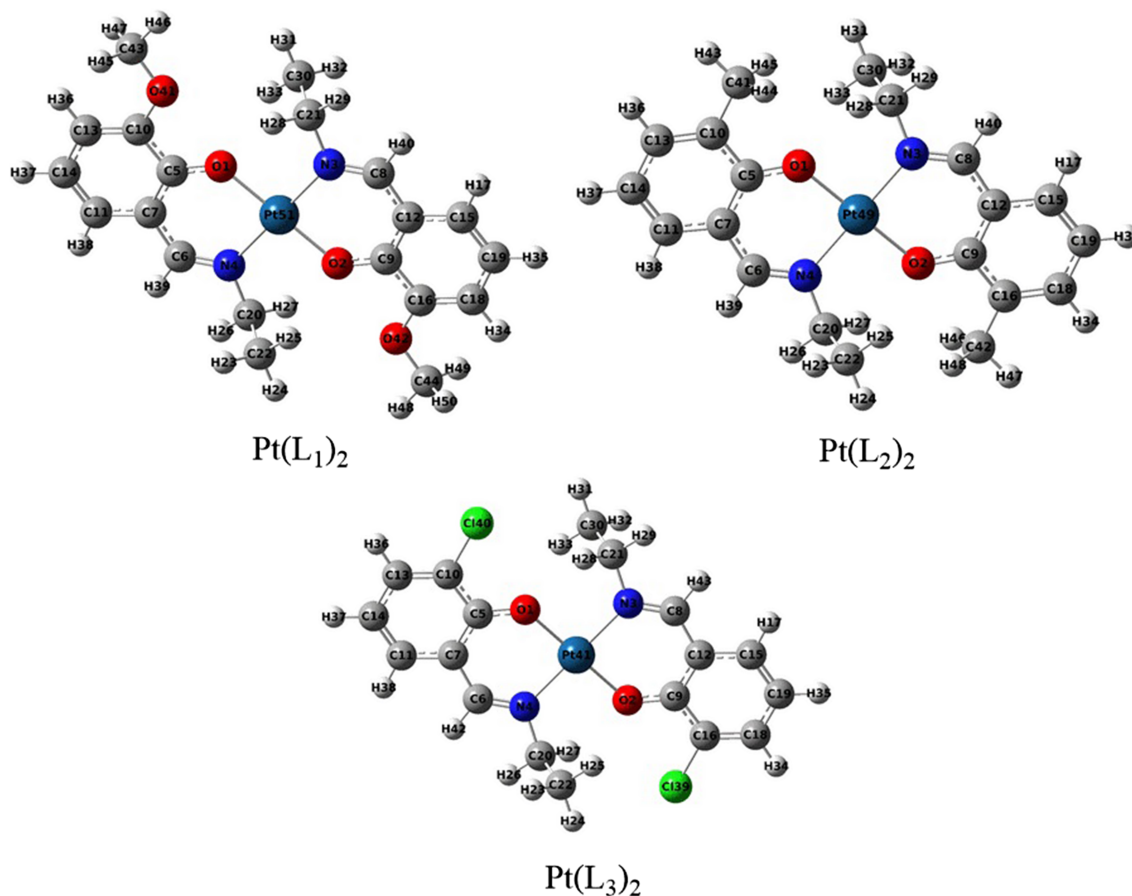
FIGURE 1   Optimized structures of Pt(L₁)₂, Pt(L₂)₂, and Pt(L₃)₂ complexes obtained at the M062X/LANL2DZ/6-31+G(d,p) level

TABLE 2   Some bond lengths and some bond angles of Pt $(L_n)_2$-type complexes computed at M062X/LANL2DZ/6-31+G(d,p) level

| Bond lengths (Å)	Pt(L₁)₂	Pt(L₂)₂	Pt(L₃)₂
Pt-N3=Pt-N4	2.044	2.046	2.045
Pt-O1=Pt-O2	2.027	2.029	2.029
N4-C6=N3-C8	1.289	1.289	1.287
N4-C20=N3-C21	1.472	1.472	1.473
C5-C10=C9-C16	1.437	1.430	1.424
C6-C7=C8-C12	1.445	1.444	1.448
C5-O1=C9-O2	1.301	1.305	1.298
Bond angles (°)	**Pt(L₁)₂**	**Pt(L₂)₂**	**Pt(L₃)₂**
O1-Pt-N4=O2-Pt-N3	91.7	91.7	91.6
O1-Pt-N3=O2-Pt-N4	88.3	88.2	88.4
O1-Pt-O2=N3-Pt-N4	180.0	180.0	180.0
Pt-O1-C5=Pt-O2-C9	126.0	126.7	126.0
Pt-N3-C8=Pt-N4-C6	123.3	123.4	123.4

3.2 | Ground state structures of the complexes

The ground state molecular structures of Pt $(L_n)_2$-type four-coordinated complexes were computed at M062X/ LANL2DZ/6-31+G(d,p) in the aqueous phase. The computed ground structures of the complexes are given in Figure 1.

Some bond lengths and some bond angles thought to be characteristic for complexes are given in Table 2.

As seen in Table 2, Pt-N bond lengths in complexes are 2.04 Å, Pt-O bond lengths are 2.03 Å, and C=N bond lengths are around 1.29 Å. These values are in agreement with similar complexes available in the literature.[41] It is also seen that the lengths of the bonds in trans positions such as Pt-N3=Pt-N4 and Pt-O1=Pt-O2 are equal.

In ideal square plane geometry, the cis angles around the central metal atom are expected to be 90° and the trans angles to be 180°. As seen in Table 2, the bond angles of O1-Pt-N4, O2-Pt-N3, O1-Pt-N3, and O2-Pt-N4, which are the angles between the donor atoms in the cis

—WILEY—

FIGURE 2 IR spectra of Pt $(L_n)_2$-type complexes calculated at M062X/ LANL2DZ/6-31+G(d,p) level in the aqueous medium
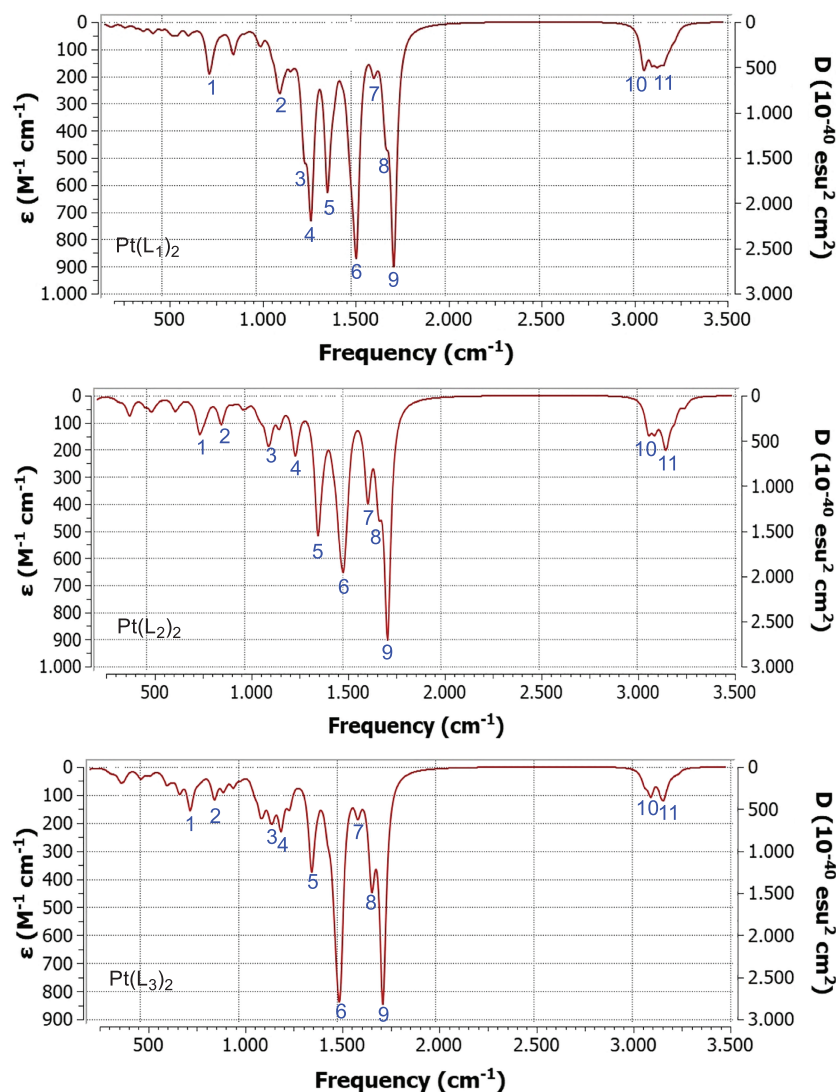
positions, are approximately 90°, and the angles between the donor atoms in the trans positions, N3-Pt-N4 and O1-Pt-O2 bond angles, were calculated as approximately 180°. Due to the inductive effects of the side groups in the ligands, the bond angles differ slightly from the bond angles of the ideal square plane structure. Therefore, it can be said that the complexes have a distorted square-plane geometry. In addition, these bond angles are compatible with similar complexes in the literature.[41]

3.3 | IR spectra of the complexes and labeling of peaks

IR spectra of Pt $(L_n)_2$-type complexes were calculated at M062X/LANL2DZ/6-31+G(d,p) level in an aqueous medium. IR spectra are given in Figure 2, and the labeling of the peaks thought to be characteristic for the complexes is given in Table 3.

The frequencies in Table 3 are harmonic. The anharmonic frequencies are calculated by multiplying the harmonic frequencies with the appropriate scale factor for each calculation level. Scale factors for various levels are in the range of 0.8–1 in the literature.[42] In the literature, a scale factor of the calculation level used in this study was not found. However, the scale factor for M062X/ LANL2DZ, which is close to the calculation level we used, is 0.952.[43]

In IR spectroscopy, the 650–1250 cm^{-1} region, called the fingerprint region, is not very distinctive. The description of the spectrum in this region is often not fully structured due to its complexity. On the other hand, if the fingerprint region can be explained, important information can be obtained since it is a characteristic for each substance. As seen in Table 3, generally C-H and C-C-C angle bending vibrations were observed in this region. For all three complexes, peaks of asymmetric $C_{ar}\text{-}O_d$ vibration were observed around 1370 and 1520 cm^{-1}.

TABLE 3 Labeling of the peaks observed in the IR spectrum of Pt $(L_n)_2$-type complexes in the aqueous medium calculated at M062X/ LANL2DZ/6-31+G(d,p) level

	Peak no.	Mode no.	Freq. (cm^{-1})	Labeling
Pt(L$_1$)$_2$	1	50	750.9	ω (C$_{ar}$-H)
	2	75	1129.7	α (C$_{ar}$-H)
	3	87	1256.2	γ (C$_{ar}$-H)
	4	89	1291.5	ν_{as} (C$_{ar}$-O)
	5	94	1379.3	ν_{as} (C$_{ar}$-O$_d$), γ (C$_{ar}$-H)
	6	116	1533.0	ν_{as} (C$_{ar}$-C$_{ar}$), ν_{as} (C$_{ar}$-O$_d$)
	7	118	1624.5	ν_{as} (C$_{ar}$-C$_{ar}$)
	8	120	1687.5	ν_{as} (C$_{ar}$-C$_{ar}$)
	9	122	1730.7	ν_{as}(C=N)
	10	124	3053.5	ν_{as} (C$_{al}$-H)
	11	134	3162.4	ν_{as} (C$_{al}$-H), ν_{as}(C-H)$_{imine}$
Pt(L$_2$)$_2$	1	48	771.1	ω (C$_{ar}$-H)
	2	54	881.2	δ (C$_{ar}$-C$_{ar}$-C$_{ar}$)
	3	73	1118.1	α (C$_{ar}$-H)
	4	81	1258.9	ν_{as} (C$_{ar}$-C$_{ar}$), γ (C$_{ar}$-H)
	5	88	1375.4	ν_{as} (C$_{ar}$-O$_d$), γ (C$_{ar}$-H)
	6	110	1521.6	ν_{as} (C$_{ar}$-C$_{ar}$), ν_{as} (C$_{ar}$-O$_d$)
	7	112	1628.0	ν_{as} (C$_{ar}$-C$_{ar}$)
	8	114	1684.1	ν_{as} (C$_{ar}$-C$_{ar}$)
	9	116	1729.8	ν_{as}(C=N)
	10	122	3090.7	ν_{as} (C$_{al}$-H)
	11	129	3144.9	ν_{as} (C$_{al}$-H), ν_{as}(C-H)$_{imine}$
Pt(L$_3$)$_2$	1	46	756.3	ω (C$_{ar}$-H)
	2	52	880.4	δ (C$_{ar}$-C$_{ar}$-C$_{ar}$)
	3	71	1164.6	α (C$_{ar}$-H), α (C$_{al}$-H)
	4	75	1218.4	γ (C$_{ar}$-H)
	5	84	1375.8	ν_{as} (C$_{ar}$-O$_d$), γ (C$_{ar}$-H)
	6	98	1520.8	ν_{as} (C$_{ar}$-C$_{ar}$), ν_{as} (C$_{ar}$-O$_d$)
	7	100	1607.9	ν_{as} (C$_{ar}$-C$_{ar}$)
	8	102	1678.5	ν_{as} (C$_{ar}$-C$_{ar}$)
	9	104	1735.7	ν_{as}(C=N)
	10	108	3095.6	ν_{as} (C$_{al}$-H)
	11	112	31160.6	ν_{as} (C$_{al}$-H), ν_{as}(C-H)$_{imine}$

Notes: ν_{as}, asymmetric stretching; γ, rocking; ω, wagging; α, scissoring; δ, bending; al, aliphatic; ar, aromatic; d, donor.

The peaks of aromatic C=C bond stretching vibrations are observed around 1500 and 1600 cm^{-1}. Peaks 6, 7, and 8 in complexes show C=C vibrations. It was observed at the expected frequency.

The characteristic C=N stretching peak of Schiff bases is observed in the region of 1600–1700 cm^{-1}. The peaks numbered 9 in the IR spectra belong to the C=N asymmetric stretching vibrations. The peaks belonging to the C=N group in the Pt(L$_1$)$_2$, Pt(L$_2$)$_2$, and Pt(L$_3$)$_2$ complexes were calculated as 1730.7, 1729.7, and 1735.6 cm^{-1}. When these frequencies are multiplied by a value between 0.8 and 1 (scale factor), they correspond to the range of 1600–1700 cm^{-1}. This indicates that the calculated frequencies are in the expected region.

Aliphatic C-H and imine C-H stretching vibrations are observed in the 2850–3100 cm^{-1} region. Peaks 10 and 11 in Pt (L$_n$)$_2$-type complexes belong to C-H stretching vibrations. According to the fundamental equation of

FIGURE 3 ^{1}H-NMR spectra of Pt $(L_n)_2$-type complexes calculated at M062X/LANL2DZ/6-31+G(d,p) level by gauge-independent atomic orbitals (GIAO) method in the aqueous medium
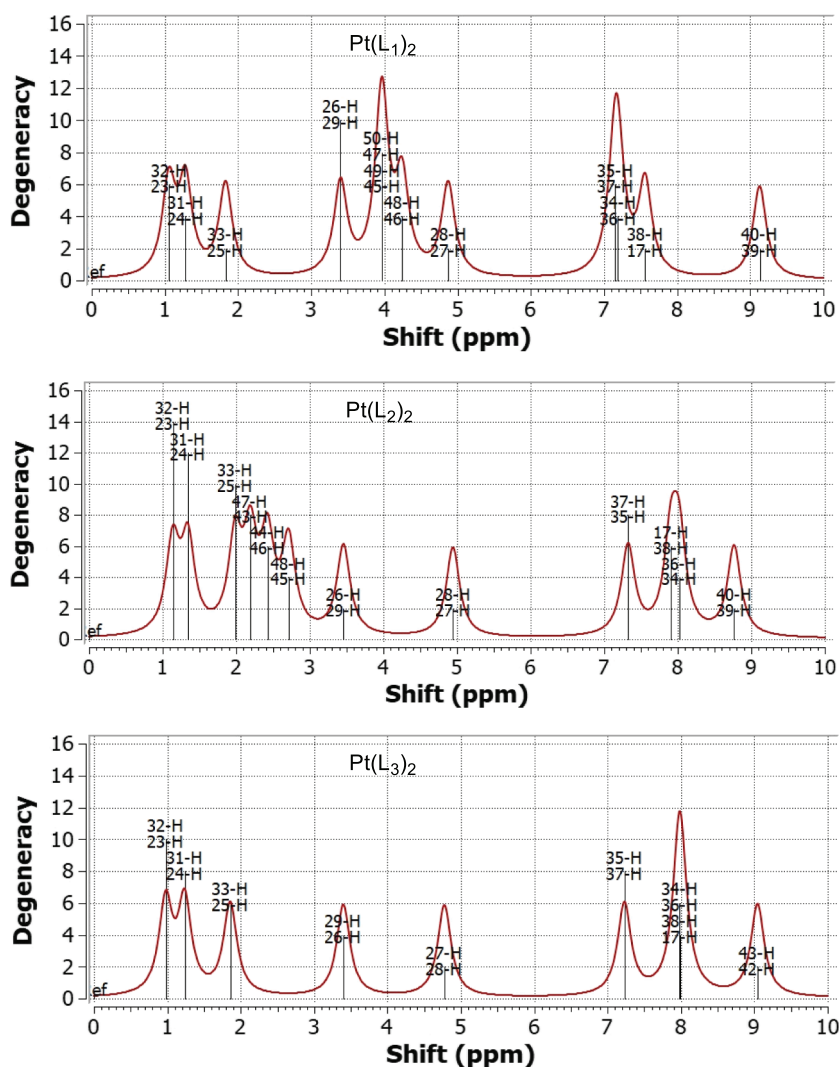
vibrational frequency, C-H vibrations are obtained at high frequencies, since the reduced mass of the C-H bonds is small.

3.4 | NMR spectra of the complexes and labeling of peaks

NMR spectra and chemical shift values of the complexes were calculated by GIAO method in the aqueous phase at the level of M062X/LANL2DZ/6-31+G(d,p). Tetramethyl silane (TMS) was used as a reference. In the aqueous phase for TMS, ^{1}H-NMR chemical shift value was computed as 31.74 ppm and the ^{13}C-NMR chemical shift was 197.25 ppm. The calculated ^{1}H-NMR spectra of the complexes are given in Figure 3.

When Figure 3 is examined, it is seen that the Pt$(L_1)_2$ and Pt$(L_2)_2$ complexes contain 12 equivalents of protons and the Pt$(L_3)_2$ complex contains nine equivalents of protons. These numbers are also the number of hydrogen

atoms present in L_n ligands. This result shows that the protons in the L_n ligands are not equivalent. The fact that there are two molecules of these ligands in the complexes and that the same number of ^{1}H-NMR peaks are observed shows that the molecular structures of the complexes are distorted square planar, because there are trans and cis positions to each other in the square planar structure. Protons in the trans and cis positions are interchanged by rotation around a C_2 axis. Therefore, they are equivalent protons. Equivalent protons peak at the same chemical shift value. The ^{1}H-NMR chemical shifts calculated in the aqueous medium are given in Table 4.

H39, H40 protons in Pt$(L_1)_2$ and Pt$(L_2)_2$ complexes and H42, H43 protons in Pt$(L_3)_2$ complexes have the highest chemical shift values. When Figure 1 is examined, it is seen that these protons are located in the azomethine (H-C=N) group. The carbon atom in the azomethine group has both sp^2 hybridization and is bonded to the nitrogen atom, which has a higher electronegativity. Therefore, the H-C=N proton is less shielded.

Pt(L$_1$)$_2$	δ (ppm)	Pt(L$_2$)$_2$	δ (ppm)	Pt(L$_3$)$_2$	δ (ppm)
H23=H32	1.05	H23=H32	1.14	H23=H32	0.98
H24=H31	1.28	H24=H31	1.34	H24=H31	1.24
H25=H33	1.83	H43=H47	1.99	H25=H33	1.86
H26=H29	3.40	H25=H33	2.19	H26=H29	3.40
H45=H49	3.96	H44=H46	2.42	H27=H28	4.78
H47=H50	3.97	H45=H48	2.71	H35=H37	7.23
H46=H48	4.24	H26=H29	3.46	H17=H38	7.98
H27=H28	4.87	H27=H28	4.94	H34=H36	7.99
H34=H36	7.15	H35=H37	7.33	H42=H43	9.04
H35=H37	7.19	H17=H38	7.91		
H17=H38	7.56	H34=H36	8.02		
H39=H40	9.13	H39=H40	8.77		

TABLE 4 ^{1}H-NMR chemical shifts (ppm) of Pt (L$_n$)$_2$-type complexes calculated by GIAO method in the aqueous phase at M062X/LANL2DZ/6-31+G(d,p) level

Abbreviation: GIAO, gauge-independent atomic orbitals.
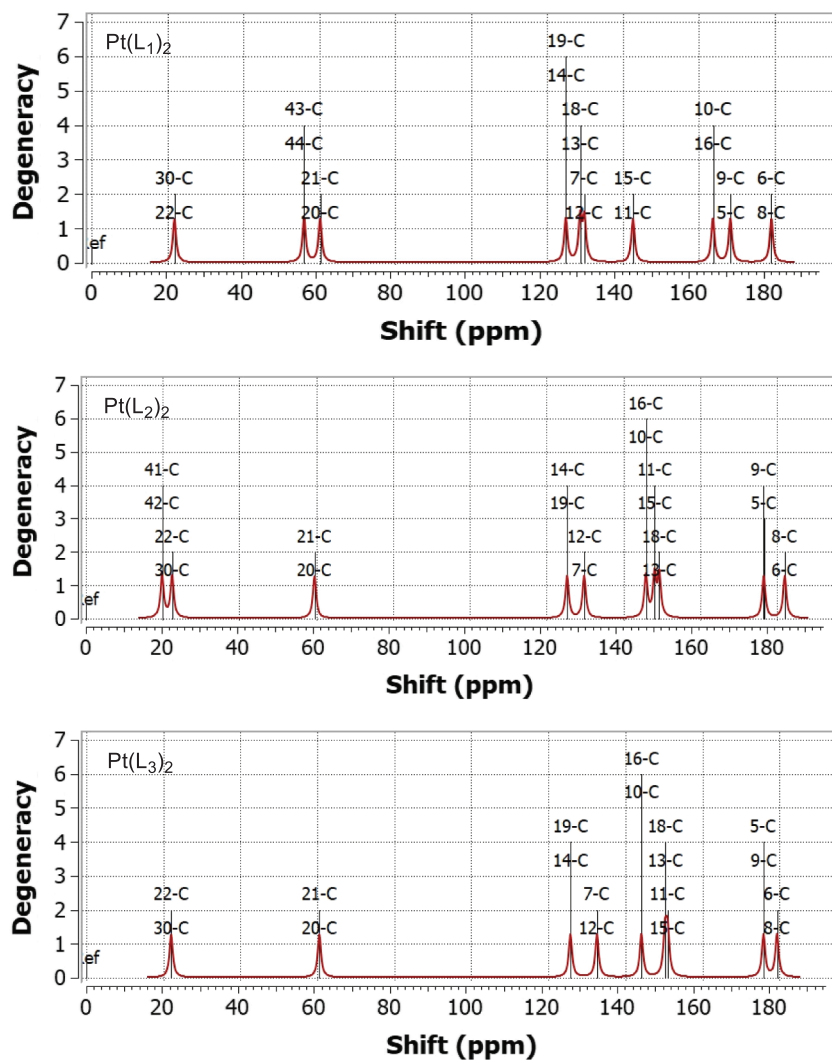
FIGURE 4 ^{13}C-NMR spectra of Pt (L$_n$)$_2$-type complexes calculated by gauge-independent atomic orbital (GIAO) method in the aqueous phase at M062X/LANL2DZ/6-31+G(d,p) level

TABLE 5 ^{13}C-NMR chemical shift values (ppm) of Pt (L$_n$)$_2$-type complexes calculated by GIAO method in the aqueous phase at M062X/LANL2DZ/6-31+G(d,p) level

Pt(L$_1$)$_2$	δ (ppm)	Pt(L$_2$)$_2$	δ (ppm)	Pt(L$_3$)$_2$	δ (ppm)
C22=C30	21.9	C41=C42	19.8	C22=C30	22.0
C43=C44	56.1	C22=C30	22.4	C20=C21	60.5
C20=C21	60.3	C20=C21	59.5	C14=C19	125.7
C14=C19	125.0	C14=C19	125.4	C7=C12	132.6
C13=C18	128.8	C7=C12	129.8	C10=C16	144.2
C7=C12	129.9	C10=C16	145.9	C11=C15	150.3
C11=C15	142.7	C11=C15	148.1	C13=C18	151.0
C10=C16	163.8	C13=C18	149.4	C5=C9	175.9
C5=C9	168.4	C5=C9	176.6	C6=C8	179.4
C6=C8	179.2	C6=C8	182.0		

Abbreviation: GIAO, gauge-independent atomic orbitals.

Less shielded protons come out at high ppm. In all three complexes, H23, H32 protons peaked at the lowest ppm value. When Figure 1 is examined, it is seen that these protons are in the alkyl group. The alkyl group carbons are sp[3] hybridized, and the s-character is low. In addition, these protons do not feel the inductive effect of electronegative atoms, because they are far away from electronegative atoms such as N and O. For these reasons, proton nuclei are highly shielded by their electrons and peak at low ppm.

OCH$_3$ protons attached to the aromatic ring in the Pt(L$_1$)$_2$ complex are labeled with H45, H46, H47, H48, H49, and H50. Chemical shift values are in the range of 3.81–4.24 ppm. Chemical shift values labeled as H23, H24, and H25 for the CH$_3$ protons attached to the aromatic ring in the Pt(L$_2$)$_2$ complex are in the range of 1.08–2.29 ppm. The chemical shift values of the aromatic ring hydrogens H17, H34, H35, H36, H37, and H38 in all three complexes were found in the range of 6.82–8.2 ppm.

^{13}C-NMR spectra of Pt (L$_n$)$_2$ complexes calculated in the aqueous phase at the level of M062X/LANL2DZ/6-31+G(d,p) by GIAO method are given in Figure 4.

When ^{13}C-NMR spectra in Figure 4 are examined, it is seen that there are 10 equivalent carbon atoms in the Pt(L$_1$)$_2$ and Pt(L$_2$)$_2$ complexes and nine equivalents in the Pt(L$_3$)$_2$ complex. This result can be interpreted as the interpretation of ^{1}H-NMR spectra and indicates that structures of the complexes are distorted square planar. The chemical shift values of Pt (L$_n$)$_2$-type complexes in the aqueous phase calculated by the GIAO method at the level of M062X/LANL2DZ/6-31+G(d,p) are given in Table 5.

As seen is Table 5, the highest chemical shift values were obtained for C6 and C8 in all three complexes. As can be seen in Figure 1, these carbon atoms are in the
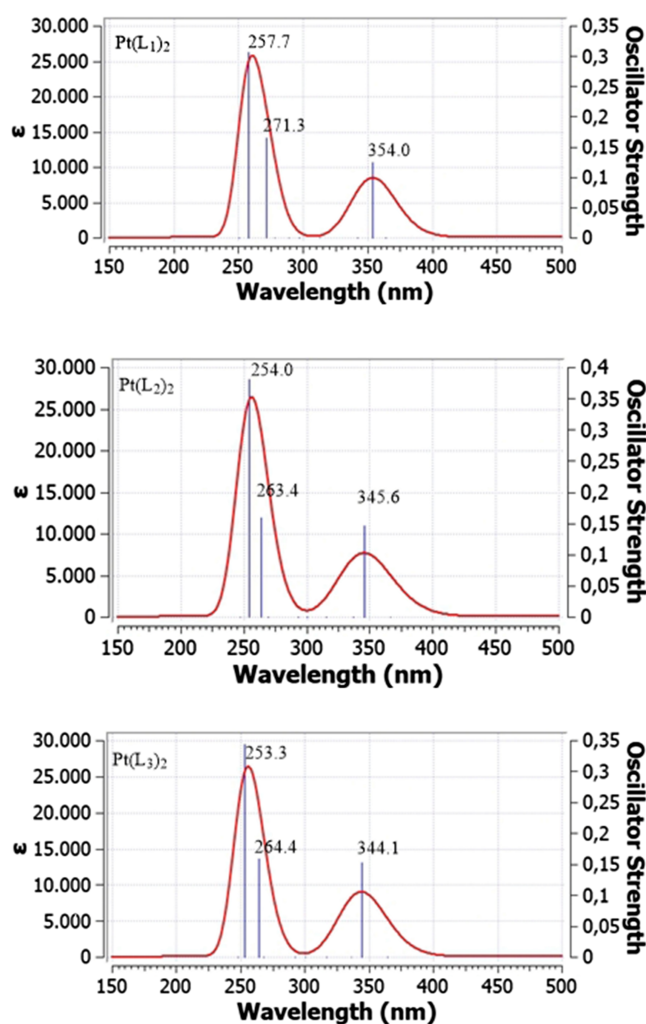
FIGURE 5 Calculated UV–Vis spectra of Pt (L$_n$)$_2$-type complexes in the aqueous medium at TD-M062X/LANL2DZ/6-31+G(d,p) level

azomethine (H-C=N) groups. Carbon atoms in azomethine groups have a high s-character and are attached to a nitrogen atom with high electronegativity. This
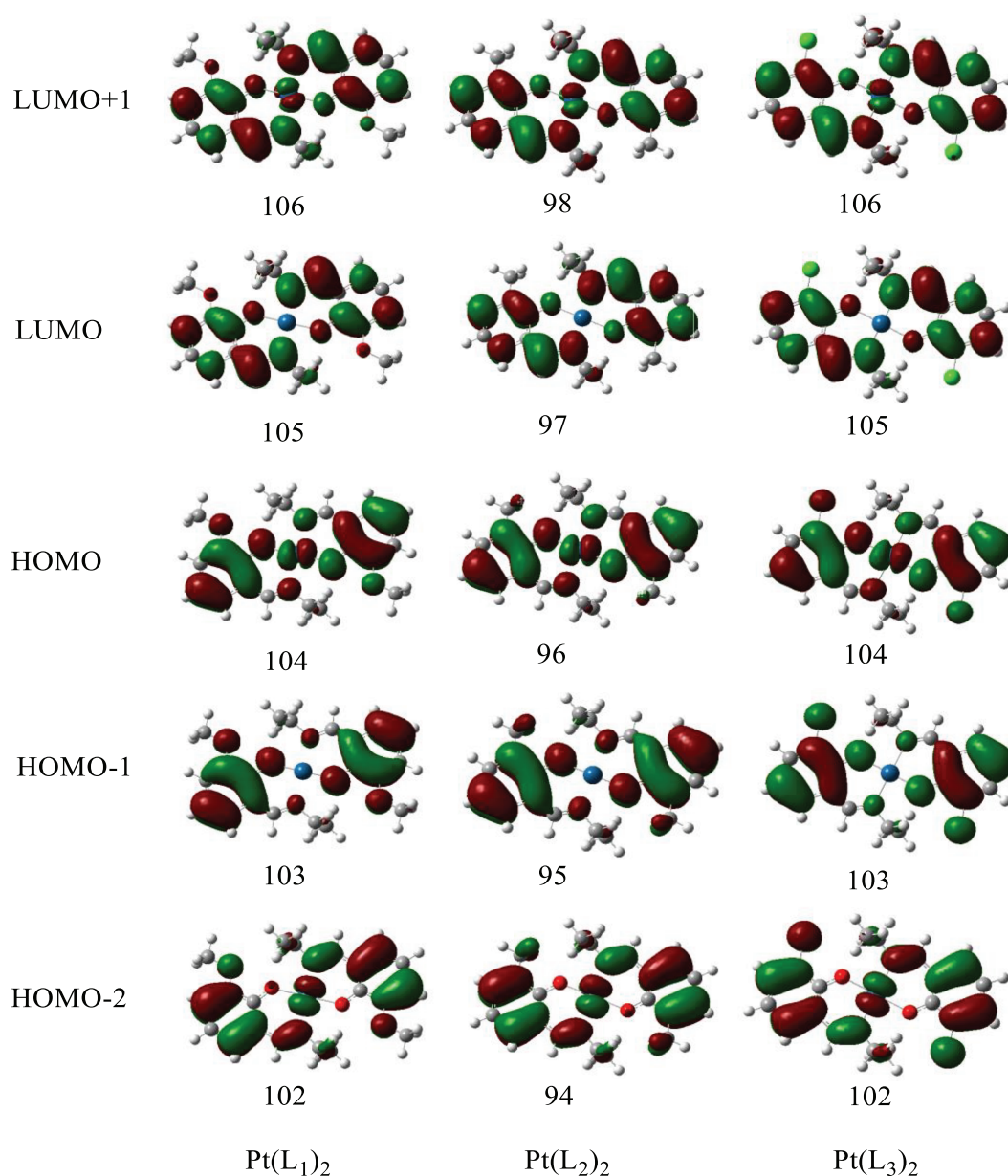
LUMO+1		
106	98	106
LUMO		
105	97	105
HOMO		
104	96	104
HOMO-1		
103	95	103
HOMO-2		
102	94	102
$Pt(L_1)_2$	$Pt(L_2)_2$	$Pt(L_3)_2$

FIGURE 6   Contour diagrams of frontier orbitals for Pt $(L_n)_2$-type complexes

causes less shielding of the carbon nucleus. Less shielded nucleus peaks at high ppm.

C22, C30 carbons in $Pt(L_1)_2$ and $Pt(L_3)_2$ complexes and C41, C42 carbons in $Pt(L_2)_2$ complex peaked at the lowest ppm value. As seen in Figure 1, these carbon atoms are alkyl carbons located far from electronegative atoms. C5, C7, C9, C10, C11, C12, C13, C14, C15, C16, C18, and C19 carbons are in the aromatic rings. They have smaller chemical shifts than the azomethine carbons. The chemical shift values of aromatic ring carbons are in the range of 125–177 ppm, and their chemical shift values change depending on their proximity to the electronegative atom. Since the C5 and C9 carbons are adjacent to the electronegative oxygen atom, they have a

higher chemical shift than the other aromatic ring carbons. C20, C21, C22, and C30 carbons are aliphatic carbons; they have sp³ hybridization and have a low chemical shift value since their s-characters are low. These findings are in agreement with the values in similar complexes given in the literature.[44]

3.5 | UV–Vis spectra of the complexes and assignment of bands

UV–Vis spectra of the platinum complexes were calculated in the aqueous phase at the level of TD-DFT/M062X/LANL2DZ/6-31+G(d,p). The default setting of

FIGURE 7 Molecular electrostatic potential (MEP) maps of the complexes obtained at M062X/LANL2DZ/6-31+G(d,p) level

$Pt(L_1)_2$ $Pt(L_2)_2$ $Pt(L_3)_2$

-0.04   +0.04
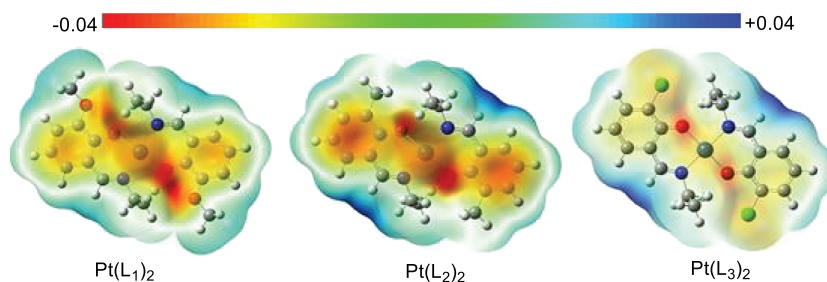
the Gaussian 09 program was used in the TD-DFT calculations. The default settings of Gaussian 09 include Nstate = 6, root = 1. Here, Nstate = 6 shows that six electronic states are considered in TD-DFT calculations and three of them are singlet states and the other three are triplet states. Root = 1 indicates the first excited state. UV–Vis spectra of the complexes calculated under the specified conditions are given in Figure 5.

As can be seen from Figure 5, two bands are formed in the electronic spectrum of each complex. UV–Vis spectrum of the $Pt(L_1)_2$ complex is slightly different from the spectrum of $Pt(L_2)_2$ and $Pt(L_3)_2$ complexes in terms of wavelengths. It is seen that the low wavelength band consists of two peaks, and the higher wavelength band consists of one peak.

To predict electronic transitions that reveal bands in the electronic spectrum, the excitation coefficients in the computational output files were examined and the transitions with the highest transition coefficients were evaluated. In general, it was predicted that the lower wavelength bands emerge from the transitions between HOMO-2→LUMO and HOMO-1→LUMO+1 orbitals, while the higher wavelength bands consist of transitions between HOMO→LUMO orbitals. The characters of HOMO-2, HOMO-1, HOMO, LUMO, and LUMO+1 can be predicted from the contour diagrams. For this reason, contour diagrams of the frontier orbitals for the complexes were obtained and given in Figure 6.

As can be seen from Figure 6, in general, in all complexes, HOMO-2 and HOMO-1 show the π-molecular orbitals in the benzene ring, and LUMO and LUMO+1 show the π*-molecular orbitals in the benzene ring. According to this evaluation, it can be said that HOMO-2→LUMO and HOMO-1→LUMO+1 transitions are predominantly π→π* transitions. As can be seen from the HOMO contour diagram, the benzene ring π-molecular orbitals, central metal atom d orbitals, donor oxygen, and donor nitrogen orbitals make the most contributions to the HOMO orbital. So, the HOMO→LUMO transition is also a M→LCT transition in addition to the π→π* transition.

## 3.6 | Molecular electrostatic potential (MEP) maps of the complexes

To predict the electropositive and electronegative regions of the complexes, the MEP map was calculated at M062X/LANL2DZ/6-31+G(d,p) level in the aqueous phase and is given in Figure 7.

In these maps, the red color shows the regions with high electron density and the blue color shows the regions with low electron density. As can be seen from Figure 7, the blue color intensity in the MEP map of the $Pt(L_1)_2$ complex is lower than that of the $Pt(L_2)_2$ and $Pt(L_3)_2$ complexes. This finding indicates that the nucleophilicity of the $Pt(L_1)_2$ complex is higher than that of the $Pt(L_2)_2$ and $Pt(L_3)_2$ complexes. This result may be closely related to the fact that the CH_3O group in Schiff base ligands is electron-withdrawing group (EWG) and the CH_3 and Cl are electron donor group (EDG).

3.7 | Molecular orbital energy diagrams (MOED)

MOED of the investigated platinum complexes were calculated at M062X/LANL2DZ/6-31+G(d,p) level in the aqueous medium. The energy diagrams of the molecular orbitals between HOMO-2 and LUMO+1 were given in Figure 8.

As seen in Figure 8, the frontier orbitals HOMO and LUMO are given in yellow. The 104th and 105th molecular orbitals respectively are HOMO and LUMO for $Pt(L_1)_2$ and $Pt(L_3)_2$ complexes whereas 96th ve 97th molecular orbitals are HOMO and LUMO for $Pt(L_2)_2$. The energy and symmetry of each molecular orbital are given next to it. Energies are in Hartree units. One Hartree is 27.2116 eV. All of the molecular orbitals appear to be of the "a" symmetry type. This type of symmetry shows that the molecule does not contain any symmetry operations; that is, it is an asymmetric molecule. Since the molecules are not in a regular square plane, the symmetry elements are eliminated. HOMO and LUMO
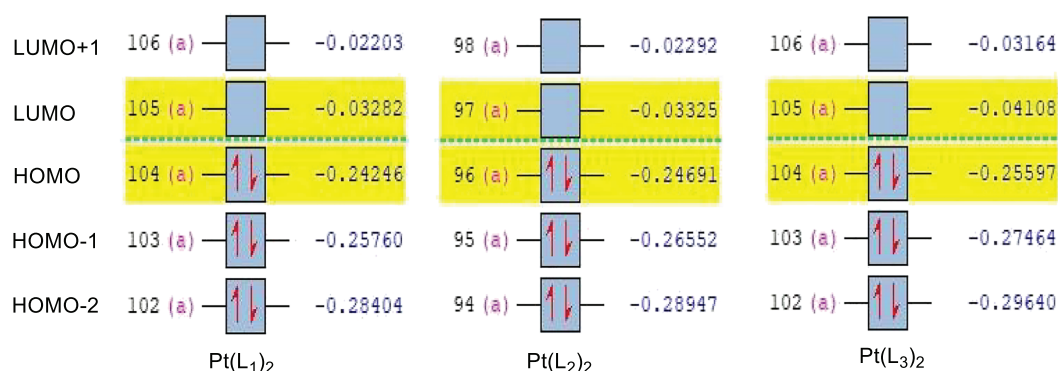
FIGURE 8 Molecular orbital energy diagrams of Pt $(L_n)_2$ complexes computed at M062X/LANL2DZ/6-31+G(d,p) level in the aqueous medium

TABLE 6 Some molecular properties for Pt(L$_1$)$_2$, Pt(L$_2$)$_2$, Pt(L$_3$)$_2$, cisplatin, and SHA computed at M062X/LANL2DZ/6-31+G(d,p) level in the water phase

Descriptors	Pt(L$_1$)$_2$	Pt(L$_2$)$_2$	Pt(L$_3$)$_2$	Cisplatin	SHA
E_{HOMO}[a]	−6.598	−6.719	−6.965	−8.510	−7.338
E_{LUMO}[a]	−0.893	−0.905	−1.118	−0.596	−0.952
I[a]	6.598	6.719	6.965	8.510	7.338
A[a]	0.893	0.905	1.118	0.596	0.952
ΔE[a]	5.705	5.814	5.848	7.913	6.385
η[a]	2.852	2.907	2.924	3.957	3.193
χ[a]	3.745	3.812	4.042	4.553	4.145
ω[a]	2.459	2.499	2.793	2.620	2.691
μ[b]	0.001	0.001	0.003	11.176	1.652
α[c]	441.323	430.949	429.981	108.345	241.396

[a]eV.

[b]Debye.

[c]a.u.

energy order of the complexes are the same, and they are Pt(L$_1$)$_2$>Pt(L$_2$)$_2$>Pt(L$_3$)$_2$.

3.8 | Some molecular properties of the complexes

Ionization potential (I), electron affinity (A), energy gap (ΔE), hardness (η), electronegativity (χ), electrophilicity index (ω) of Schiff base-platin complexes, antitumor drug cisplatin, and antibacterial standard SHA [N-(Salicylidene)-2-hydroxyaniline] were calculated from Equations 1–6. The energy of the HOMO (E_{HOMO}), energy of the LUMO (E_{LUMO}), static dipole moment (μ), and mean linear polarizability (α) were taken from the computation output files. The calculated values of these molecular properties at the level of M062X/LANL2DZ/6-31+G(d,p) in water are given in Table 6.

TABLE 7 Comparison of the relationships between Pt(L$_1$)$_2$, Pt(L$_2$)$_2$, and Pt(L$_3$)$_2$ complexes and molecular descriptors of cisplatin and SHA

Descriptor	Comparison with cisplatin
$I, \Delta E, \eta, \chi, \omega$	Pt(L$_1$)$_2$<Pt(L$_2$)$_2$<Pt(L$_3$)$_2$<Cisplatin
A	Pt(L$_1$)$_2$<Pt(L$_2$)$_2$<Cisplatin<Pt(L$_3$)$_2$
μ	Pt(L$_1$)$_2$=Pt(L$_2$)$_2$=Pt(L$_3$)$_2$<Cisplatin
α	Cisplatin<Pt(L$_3$)$_2$<Pt(L$_2$)$_2$<Pt(L$_1$)$_2$
Descriptor	Comparison with SHA
$I, \Delta E, \eta$	Pt(L$_1$)$_2$<Pt(L$_2$)$_2$<Pt(L$_3$)$_2$<SHA
A	SHA<Pt(L$_1$)$_2$<Pt(L$_2$)$_2$<Pt(L$_3$)$_2$
χ	Pt(L$_1$)$_2$<Pt(L$_2$)$_2$<SHA<Pt(L$_3$)$_2$
ω	Pt(L$_1$)$_2$<SHA<Pt(L$_2$)$_2$<Pt(L$_3$)$_2$
μ	Pt(L$_1$)$_2$=Pt(L$_2$)$_2$=Pt(L$_3$)$_2$<SHA
α	SHA<Pt(L$_3$)$_2$<Pt(L$_2$)$_2$<Pt(L$_1$)$_2$

As seen in Table 6, the values of χ, η, ΔE, A, I, and ω parameters of Schiff base platinum complexes in the aqueous phase increase in the order of $Pt(L_1)_2 < Pt(L_2)_2 < Pt(L_3)_2$. From the MEP maps of the complexes, we determined that the nucleophilicity of the $Pt(L_1)_2$ complex was high. As can be seen from Table 6, the electrophilicity index (ω) of the $Pt(L_1)_2$ complex is lower than the others. It can be said that the electrophilicity index (ω) is inversely proportional to the nucleophilicity index (ε). In other words, if the nucleophilicity index of a substance is high, the electrophilicity index will be low.

The fact that the static dipole moments of the complexes are almost zero Debye indicates that the complexes are in disordered square plane structures. If the structures were an ideal square plane, the static dipole moment would be zero Debye.

The mean molecular polarizability of $Pt(L_2)_2$ and $Pt(L_3)_2$ complexes are very close to each other. Mean molecular polarizability is related to molecular size and softness. The mean molecular polarizability values of the $Pt(L_2)_2$ and $Pt(L_3)_2$ complexes are very close, indicating that CH_3 and Cl substituents are close in size.

In addition, the molecular properties of cisplatin, which is used as a cancer drug, and SHA, which is used as an antibacterial reference, given in Table 6, are close

to the calculated properties of platinum complexes. Comparisons between molecular structure descriptors of complexes and molecular properties of cisplatin and SHA are given in Table 7.

As seen in Table 7, the values of many molecular descriptors of the complexes are smaller than those of cisplatin and SHA, which are taken as references. The molecular descriptors of the complexes being larger or smaller than those of the references do not provide information on biological activity. Having some descriptors large and some small can increase activity. The shortest way to predict biological activity is to do molecular docking calculations.

3.9 | Estimation of anticancer and antibacterial activities of the complexes

Molecular docking calculations are one of the popular techniques used to predict the biological activities of molecules and to design drug candidate molecules. Secondary chemical interactions between the minimalized protein structure of cell lines and the drug candidate molecule can be investigated by molecular docking calculations. In this way, secondary chemical interaction types, interaction modes, and interaction energies, which is
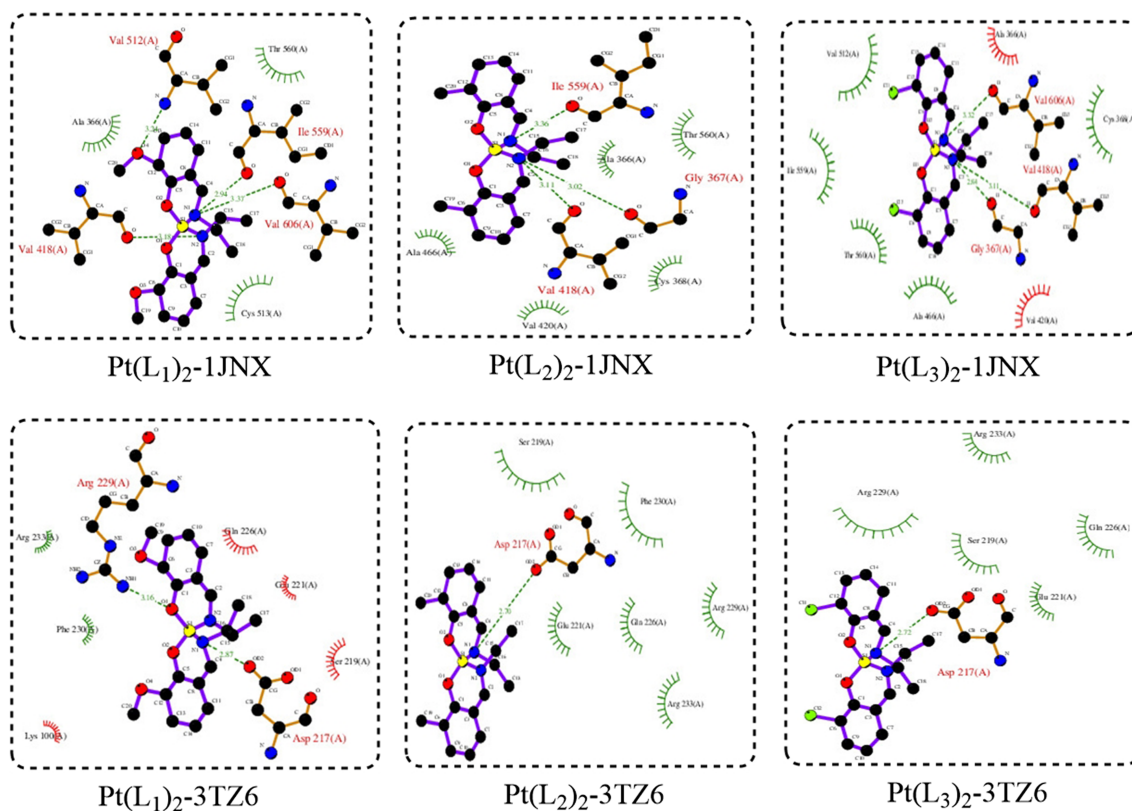

FIGURE 9 Docking poses between Pt $(L_n)_2$-type complexes and target protein cell lines

called the binding energy, between the target protein and the drug candidate molecule can be computed.

In this research, the complexes optimized in the aqueous phase were docked against the breast cancer cell line MCF-7 (PDB ID:1JNX) and the tuberculosis bacterial cell line H37Rv (PDB ID: 3TZ6). Information on these cell lines was given in our previous study on HL_n ligands.[9] Docking Server was used for docking process.[39] Geometry optimization of the complexes on the docking server was done again with the MMFF94 method. The Gasteiger partial load calculation method was chosen. pH = 7.0 was taken. Grid maps were created using $90 \times 90 \times 90$ Å grid points and 0.2 Å spacing. Lamarckian genetic algorithm was used for insertion simulations. The population size was set to 150. The 5 Å quaternion and torsion steps were applied for the studied complexes to search for the appropriate region of the target protein. Docking poses of Pt $(L_n)_2$ complexes against MCF-7 (PDB ID: 1JNX) and H37Rv (PDB ID: 3TZ6) cell lines are presented in Figure 9, and the interaction types between Pt $(L_n)_2$-type complexes and cell lines of target proteins are presented in Table 8.

As can be seen in Table 8, there are more types of interactions between the $Pt(L_3)_2$ complex and the 1JNX than both the reference and other complexes. $Pt(L_3)_2$ complex formed hydrophobic interactions with amino acids CYS368, ALA366, CYS513, and VAL420 of the 1JNX protein; H bond interactions with GLY367, ILE559, VAL606, and VAL418; and halogen bond interactions with VAL512. Cisplatin, taken as a reference, made H bond interactions with VAL606, ILE559, and GLY367. This result shows that $Pt(L_3)_2$ complex may be more active than other complexes against MCF-7 (PDB ID: 1JNX) breast cancer cell line.

Interaction types of Pt $(L_n)_2$-type complexes with H37Rv (PDB ID: 3TZ6) *Mycobacterium tuberculosis* bacteria cell line are also given in Table 8. As seen in Table 8, the $Pt(L_3)_2$ complex had hydrophobic interaction with the amino acids PHE230 and PRO239 of the 3TZ6 protein and polar interaction with ARG233. The reference SHA, on the other hand, made hydrophobic interactions with PHE230, polar interactions with ARG233, and pi-pi interactions with PHE230.

To predict anticancer and antibacterial activities of Pt $(L_n)_2$-type complexes against 1JNX and 3TZ6 proteins, binding energies (BE), intermolecular energies (IE), the sum of interactions of van der Waals, H bond, dissolve energies (WHDE), interaction surfaces (IS), and inhibition constants (Ki) were calculated for platinum complexes and standards. Docking parameters of Pt $(L_n)_2$ complexes and standards are given in Table 9. Values in parentheses are for HL_n ligands and are taken from Kaya et al.[9] to compare the anticancer and antibacterial activities of Pt $(L_n)_2$ complexes with HL_n ligands.

TABLE 8 Types of interactions between the complexes and the 1JNX and 3TZ6 target protein cell lines

	Hydrophobic	Polar	pi-pi	H bonds	Halogen bond
$Pt(L_1)_2$-1JNX	ALA366 ALA466 ILE559 ALA607 CYS513	-	-	VAL606 VAL418	-
$Pt(L_2)_2$-1JNX	VAL606 CYS513 ALA466 ALA366	-	-	GLY367 VAL418 ILE559	-
$Pt(L_3)_2$-1JNX	CYS368 ALA366 CYS513 VAL420	-	-	GLY367 ILE559 VAL606 VAL418	VAL512
Cisplatin-1JNX	-	-	-	VAL606 ILE559 GLY367	-
$Pt(L_1)_2$-3TZ6	PHE230	ARG229 GLN226 GLU221	-	ASP217	-
$Pt(L_2)_2$-3TZ6	PHE230	ARG233	-	PRO239	-
$Pt(L_3)_2$-3TZ6	PRO239 PHE230	ARG233	-	-	-
SHA-3TZ6	PHE230	ARG233	PHE230	-	-

TABLE 9 Docking parameters showing the interaction of complexes with 1JNX and 3TZ6 target proteins

	BE[a]	IE[a]	WHDE[a]	IS	Ki[b]
$Pt(L_1)_2$-1JNX	−8.69 (−3.74)	−9.60 (−4.35)	−9.23 (−4.31)	738.76 (439.89)	425.76 (1800.0)
$Pt(L_2)_2$-1JNX	−8.75 (−4.59)	−9.35 (−5.49)	−9.15 (−5.29)	739.08 (440.74)	384.00 (431.15)
$Pt(L_3)_2$-1JNX	−9.90 (−4.69)	−10.43 (−5.56)	−10.18 (−5.34)	744.75 (444.86)	55.61 (382.48)
Cisplatin-JNX	−2.30	−2.30	−1.81	151.94	2062.00
$Pt(L_1)_2$-3TZ6	−4.21 (−3.74)	−4.39 (−4.24)	−5.19 (−4.23)	580.66 (407.22)	826.88 (1820.0)
$Pt(L_2)_2$-3TZ6	−5.35 (−4.38)	−5.87 (−5.26)	−6.01 (−5.13)	521.10 (471.68)	119.03 (612.00)
$Pt(L_3)_2$-3TZ6	−5.83 (−4.40)	−6.41 (−4.86)	−6.55 (−4.82)	399.41 (469.43)	53.41 (598.76)
SHA-3TZ6	−3.61	−3.93	−3.97	272.60	716.81

Abbreviations: BE, binding energies; IE, intermolecular energies; IS, interaction surfaces; Ki, inhibition constants; WHDE the sum of interactions of van der Waals, H bond, dissolve energies.

[a]Kcal/mol.

[b]μM in unit; data in parentheses refer to HL_1, HL_2, and HL_3 Schiff bases.

As seen in Table 9, BE, IE, and WHDE values between the complexes and 1JNX and 3TZ6 target proteins are lower than those of the references and HL_n ligands. A lower energy value indicates higher interaction between the two species. These results indicate that the complexes interact more strongly with both 1JNX and 3TZ6 than standard substances and HL_n ligands. According to the calculated BE, IE, and WHDE, the investigated complexes could be drug candidate molecules against both the breast cancer cell line and the *M. tuberculosis* cell line.

On the other hand, it is seen that the IS of Pt $(L_n)_2$-type complexes are higher than standards substances and HL_n Schiff bases. A higher IS means higher ligand–protein interaction and results in an increase in anticancer and antibacterial activities. It is seen that the anticancer and antibacterial activities of the complexes according to IS values are higher than those of standards and HL_n ligands.

Ki is related to the amount of drug to be used in the treatment. The smaller the Ki value, the less the amount of drug used in the treatment.[45] Ki values of the Pt $(L_n)_2$ complexes against the 1JNX protein appear to be smaller than cisplatin and HL_n ligands. This result shows that Pt $(L_n)_2$ complexes should be used less than cisplatin and HL_n ligands in the case of drugs for breast cancer. However, Ki values of the $Pt(L_1)_2$ complex against the 3TZ6 protein are greater than the reference SHA, while Ki values of $Pt(L_2)_2$ and $Pt(L_3)_2$ are smaller than the reference SHA.

In general, the antitumor and antibacterial activities of the complexes against both 1JNX and 3TZ6 increased in the order of $Pt(L_1)_2 < Pt(L_2)_2 < Pt(L_3)_2$, according to BE, IE, WHDE, IS, and Ki values. This ranking shows that the $Pt(L_3)_2$ complex has the highest antitumor and antibacterial activities. This result may be related to the

binding of the electron-donating Cl group to the meta position of the azomethine group in the $Pt(L_3)_2$ complex and the halogen bonding of Cl with VAL512. This ranking is the same as that obtained for HL_n Schiff bases.[9] In addition, the antitumor and antibacterial activities of Pt $(L_n)_2$-type complexes are higher than those of HL_n Schiff base ligands. As a result, it can be said that the designed Schiff base platinum complexes have both antitumor and antibacterial activities and that experimental activity studies should be done by synthesizing them.

4 | CONCLUSIONS

In this study, Pt $(L_n)_2$-type hypothetical complexes were designed and investigated computationally. For the complexes, the M062X/LANL2DZ/6-31+G(d,p) level was found to be the best computational level. By optimizing Pt $(L_n)_2$-type complexes in the aqueous phase, their ground state structures, spectroscopic properties (IR, ^{1}H-NMR, ^{13}C-NMR, and UV–Vis), MEP maps, and some molecular properties were calculated. To estimate the anticancer and antibacterial activities of the complexes, they were docked against breast cancer cell line (MCF7) and tuberculosis bacterial cell line (H37Rv) and compared with standard substances. From optimization and spectroscopic studies, it was determined that Pt $(L_n)_2$-type complexes have distorted square planar geometry such as cisplatin. According to the calculated docking parameters, Pt $(L_n)_2$-type complexes were found to have higher activity than substances with anticancer, antibacterial standards and HL_n Schiff bases. The binding of electron-donating substituents to the meta position of the azomethine group in Schiff bases was predicted to increase both anticancer and antibacterial activities. According to the computational findings, the designed hypothetical

Schiff base-platinum complexes have antitumor and antibacterial activities and are worthy of experimental investigation.

CONFLICT OF INTEREST

The authors declare that they have no known competing financial interests or personal relationships that could have appeared to influence the work reported in this paper.

CODE AVAILABILITY

Not applicable.

AUTHOR CONTRIBUTIONS

Serpil Kaya: the calculation of optimized molecular structures, spectroscopic properties (IR, ^{1}H-NMR, ^{13}C-NMR, and UV–Vis), molecular electrostatic potential maps, and some molecular properties of Pt(L$_1$)$_2$, Pt(L$_2$)$_2$, and Pt(L$_3$)$_2$ complexes. Sultan Erkan: docking calculation of Pt(L$_1$)$_2$, Pt(L$_2$)$_2$, and Pt(L$_3$)$_2$ complexes against MCF7 cancer cell line and H37Rv *Mycobacterium tuberculosis* cell line. Duran Karakaş: design of Pt(L$_1$)$_2$, Pt(L$_2$)$_2$, and Pt(L$_3$)$_2$ complexes and interpretation of all calculation results and writing of the article.

DATA AVAILABILITY STATEMENT

The data that support the findings of this study are available from the corresponding author upon reasonable request.

ORCID

Serpil Kaya https://orcid.org/0000-0003-3360-4735
Sultan Erkan https://orcid.org/0000-0001-6744-929X
Duran Karakaş https://orcid.org/0000-0002-6770-3726

REFERENCES

[1] W. Qin, S. Long, M. Panunzio, S. Biondi, *Molecules* **2013**, *18*(10), 12264.

[2] C. M. da Silva, D. L. da Silva, L. V. Modolo, R. B. Alves, M. A. de Resende, C. V. Martins, Â. de Fátima, *J. Adv. Res.* **2011**, *2*(1), 1.

[3] D. N. Dhar, C. L. Taploo, *J. Sci. Ind. Res.* **1982**, *41*(8), 501.

[4] R. Mladenova, M. Ignatova, N. Manolova, T. Petrova, I. Rashkov, *Eur. Polym. J.* **2002**, *38*, 989.

[5] O. M. Walsh, M. J. Meegan, R. M. Prendergast, T. Al Nakib, *Eur. J. Med. Chem.* **1996**, *31*(12), 989.

[6] Z. Gul, N. U. Din, E. Khan, F. Ullah, M. N. Tahir, *J. Mol. Struct.* **2020**, *1199*, 126956.

[7] P. Przybylski, A. W. Huczyński, K. K. Pyta, B. Brzezinski, F. Bartl, *Curr. Org. Chem.* **2009**, *13*, 13.

[8] A. J. Blake, N. R. Champness, P. Hubberstey, *Coord. Chem. Rev.* **1999**, *183*, 117.

[9] S. Kaya, S. Erkan, D. Karakaş, *Spectrochim. Acta, Part a* **2021**, *244*, 118829.

[10] D. Wu, L. Guo, S. J. Li, *J. Mol. Struct.* **2020**, *1199*, 126938.

[11] O. Kocyigit, E. Guler, *J. Inclusion Phenom. Macrocyclic Chem.* **2010**, *67*(1–2), 29.

[12] A. Y. Robin, K. M. Fromm, *Coord. Chem. Rev.* **2006**, *250*(15–16), 2127.

[13] W. M. Singh, B. C. Dash, *Pesticides* **1988**, *22*(11), 33.

[14] O. Bekircan, B. Kahveci, M. Küçük, *Turk. J. Chem.* **2006**, *30*(1), 29.

[15] M. Köse, S. Purtas, S. A. Güngör, G. Ceyhan, E. Akgün, V. McKee, *Spectrochim. Acta, Part a* **2015**, *136*, 1388.

[16] M. Ghosh, M. Layek, M. Fleck, R. Saha, D. Bandyopadhyay, *Polyhedron* **2015**, *85*, 312.

[17] J. P. Scovill, D. L. Klayman, C. F. Franchino, *J. Med. Chem.* **1982**, *25*(10), 1261.

[18] D. X. West, L. K. Pannell, *Transition Met. Chem.* **1989**, *14*(6), 457.

[19] S. Ren, R. Wang, K. Komatsu, P. Bonaz-Krause, Y. Zyrianov, C. E. McKenna, C. Csipke, Z. A. Tokes, E. J. Lien, *J. Med. Chem.* **2002**, *45*(2), 410.

[20] Z. Shokohi-Pour, H. Chiniforoshan, M. R. Sabzalian, S. A. Esmaeili, A. A. Momtazi-Borojeni, *J. Biomol. Struct. Dyn.* **2018**, *36*(2), 532.

[21] P. Ghorai, R. Saha, S. Bhuiya, S. Das, P. Brandão, D. Ghosh, T. Bhaumik, P. Bandyopadhyay, D. Chattopadhyay, A. Saha, *Polyhedron* **2018**, *141*, 153.

[22] I. B. Amali, M. P. Kesavan, V. Vijayakumar, N. I. Gandhi, J. Rajesh, G. Rajagopal, *J. Mol. Struct.* **2019**, *1183*, 342.

[23] M. Ariyaeifar, H. A. Rudbari, M. Sahihi, Z. Kazemi, A. A. Kajani, H. Zali-Boeini, N. Kordestani, G. Bruno, S. Gharaghani, *J. Mol. Struct.* **2018**, *1161*, 497.

[24] A. Bergamo, P. J. Dyson, G. Sava, *Coord. Chem. Rev.* **2018**, *360*, 17.

[25] S. Dilruba, G. V. Kalayda, *Cancer Chemother. Pharmacol.* **2016**, *77*(6), 1103.

[26] D. Lebwohl, R. Canetta, *Eur. J. Cancer* **1998**, *34*(10), 1522.

[27] M. Galanski, *Recent Pat. Anticancer Drug Discov.* **2006**, *1*(2), 285.

[28] R. Dennington, T. Keith, J. Millam, Semichem Inc., Shawnee Mission Ks. GaussView, Version, 5 **2009**.

[29] M. J. Frisch, G. W. Trucks, H. B. Schlegel, G. E. Scuseria, M. A. Robb, J. R. Cheeseman, V. B. Scalmani, B. Mennucci, G. A. Petersson, H. Nakatsuji, M. Caricato, X. Li, H. P. Hratchian, A. F. Izmaylov, J. Bloino, G. Zheng, J. L. Sonnenberg, M. Hada, M. Ehara, K. Toyota, R. Fukuda, J. Hasegawa, M. Ishida, T. Nakajima, Y. Honda, O. Kitao, H. Nakai, T. Vreven, J. A. Montgomery Jr., J. E. Peralta, F. Ogliaro, M. Bearpark, J. J. Heyd, E. Brothers, K. N. Kudin, V. N. Staroverov, R. Kobayashi, J. Normand, K. Raghavachari, A. Rendell, J. C. Burant, S. S. Iyengar, J. Tomasi, M. Cossi, N. Rega, J. M. Millam, M. Klene, J. E. Knox, J. B. Cross, V. Bakken, C. Adamo, J. Jaramillo, R. Gomperts, R. E. Stratmann, O. Yazyev, A. J. Austin, R. Cammi, C. Pomelli, J. W. Ochterski, R. L. Martin, K. Morokuma, V. G.

Zakrzewski, G. A. Voth, P. Salvador, J. J. Dannenberg, S. Dapprich, A. D. Daniels, Ö. Farkas, J. B. Foresman, J. V. Ortiz, J. Cioslowski, D. J. Fox, *Gaussian 09, Revision d. 01*, Gaussian. Inc, Wallingford CT, 201 **2009**.

[30] Ş. Güveli, N. Özdemir, T. Bal-Demirci, B. Ülküseven, M. Dinçer, Ö. Andaç, *Polyhedron* **2010**, *29*(12), 2393.

[31] E. G. Hohenstein, S. T. Chill, C. D. Sherrill, *J. Chem. Theory Comput.* **2008**, *4*(12), 1996.

[32] Y. Yang, M. N. Weaver, K. M. Merz Jr., *Chem. A Eur. J.* **2009**, *113*(36), 9843.

[33] N. Özkan, S. Erkan, K. Sayın, D. Karakaş, *Chem. Pap.* **2020**, 1.

[34] M. Cossi, V. Barone, *J. Chem. Phys.* **1998**, *109*(15), 6246.

[35] J. A. Bohmann, F. Weinhold, T. C. Farrar, *J. Chem. Phys.* **1997**, *107*(4), 1173.

[36] D. Guillaumont, S. Nakamura, *Dyes Pigm.* **2000**, *46*(2), 85.

[37] L. A. Doyle, W. Yang, L. V. Abruzzo, T. Krogmann, Y. Gao, A. K. Rishi, D. D. Ross, *Proc. Natl. Acad. Sci.* **1998**, *95*(26), 15665.

[38] J. C. Camus, M. J. Pryor, C. Médigue, S. T. Cole, *Microbiology* **2002**, *148*(10), 2967.

[39] Z. Bikadi, E. Hazai, *J. Chem.* **2009**, *1*(1), 1.

[40] T. Akitsu, *Polyhedron* **2007**, *26*(12), 2527.

[41] H. A. Rudbari, M. Khorshidifard, V. Moazam, B. Askari, N. Habibi, G. Bruno, *J. Mol. Struct.* **2016**, *1125*, 113.

[42] I. M. Alecu, J. Zheng, Y. Zhao, D. G. Truhlar, *J. Chem. Theory Comput.* **2010**, *6*(9), 2872.

[43] M. K. Assefa, J. L. Devera, A. D. Brathwaite, J. D. Mosley, M. A. Duncan, *Chem. Phys. Lett.* **2015**, *640*, 175.

[44] M. J. Rodríguez, M. I. Fernández, A. M. González-Noya, M. Maneiro, R. Pedrido, M. Vázquez, B. Donnadieu, M. R. Bermejo, *Zeitschrift für Anorganische Und Allgemeine Chemie* **2005**, *631*(11), 2161.

[45] R. Merugu, U. K. Neerudu, K. Dasa, K. V. Singh, *Int. J. Adv. Sci. Res.* **2016**, *2*(12), 191.